Supporting information

Novel methodology for anodic stripping voltammetric sensing of heavy-metal ions using $Ti_3C_2T_x$ nanoribbons

Yinhui Yi,[a,d] Yuzhi Ma,[a] Fengxiang Ai,[a] Yixuan Xia,[a] Huiyu Lin[c] and Gangbing Zhu*[a,b,c]

[a] School of the Environment and Safety Engineering, Jiangsu University, Zhenjiang, 212013, P.R.China

[b] State Key Laboratory of Electroanalytical Chemistry, Changchun Institute of Applied Chemistry, Chinese Academy of Sciences, Changchun, Jilin 130022, P.R.China

[C] Fujian Key Laboratory of Functional Marine Sensing Materials, Ocean College, Minjiang University, P.R.China

[d] Key Laboratory of Chemical Biology and Traditional Chinese Medicine Research (Hunan Normal University), Ministry of Education, Changsha, Hunan 410081, P.R.China.

*Corresponding author. Tel.: +86 511 88791800; fax.: +86 511 88791800.
E-mail address: zhgb1030@ujs.edu.cn

Experimental section

Reagents and apparatus

$CdCl_2 \cdot 2.5H_2O$, hydrofluoric acid (HF, ≥40%), KOH, KCl, $HgSO_4$, NaCl, $ZnCl_2$, $CoCl_2 \cdot 6H_2O$, $FeCl_3$, $CaCl_2$, $MgCl_2$, $CuCl_2 \cdot 2H_2O$, $MnCl_2 \cdot 4H_2O$ and $PbC_4H_6O_4 \cdot 3H_2O$ were purchased from Aladdin Biotechnology Co., Ltd (Shanghai, China). Ti_3AlC_2 (99%) powder was purchased by Forsman Technology Company (Beijing). Phosphate buffer solution (PBS, 0.1 M) was chosen as the supporting electrolyte, which was prepared with NaH_2PO_4, Na_2HPO_4 and KCl. Aqueous solution used throughout was prepared with ultrapure water which was obtained via a Millipore purification system.All the electrochemical texts were carried out at CHI 660E Electrochemical Workstation. If no specific instructions were given, the electrochemical tests were performed in PBS (0.1 M**,** pH 5.0).

Preparation of $Ti_3C_2T_x$ NR

The preparation methodology procedure of $Ti_3C_2T_x$ NR is illustrated in Scheme 1. Firstly, the as-purchased Ti_3AlC_2 (1.0 g) was slowly added into HF solution (40.0%, 30.0 mL) and gently stirred for 24 h at 40 °C to obtain $Ti_3C_2T_x$ NS solution. The $Ti_3C_2T_x$ NS product was collected after centrifugation (5000 rpm for 10 minutes) and washed with water until the pH value of supernatant reached ~7.0, then it was dried at 60 °C in vacuum. Secondly, $Ti_3C_2T_x$ NS powder (0.2 g) was added into KOH solution (6.0 $mol \cdot L^{-1}$, 25.0 mL) under continuous stirring under N_2 atmosphere for ~100 h at 25 °C. And the final $Ti_3C_2T_x$ NR product was collected after washing and dried.

Construction of electrochemical sensor for Cd^{2+}

Before further modification, GCE was successively polished with 0.3 and 0.05 μM alumina powder and rinsed with ultrapure water. After the sequential sonication in acetone and

ultrapure water, GCE was dried under N_2 gas. Via casting a definite of $Ti_3C_2T_x$ NR suspension (1.0 mg/mL) onto the GCE surface and drying with infrared lamp, $Ti_3C_2T_x$ NR/GCE was obtained. For comparison, bare GCE, $Ti_3C_2T_x$ NS/GCE, graphene oxide modified GCE (GO/GCE), carbon black modified GCE (CB/GCE) and oxidized carbon nanotube modified GCE (O-MWCNTs/GCE) was prepared via the same procedure.

Electrochemical Detection of Cd^{2+}

The electrochemical sensing of Cd^{2+} in PBS solution was divided into the following two continuous steps: (1) $Ti_3C_2T_x$ NR/GCE was immersed into PBS containing Cd^{2+} with varying concentrations by stirring within a definite accumulation time. The purpose of this step is that the electrodeposition and self-reduction of Cd^{2+} to form Cd^0 on the modified electrodes surface; and (2) the electrochemical detection of Cd^{2+} was accomplished by DPV in blank PBS solution.

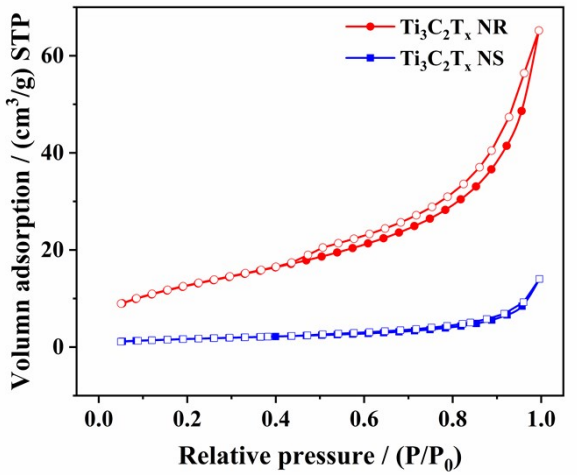

Figure S1. N_2 adsorption–desorption of $Ti_3C_2T_x$ NS and $Ti_3C_2T_x$ NR.

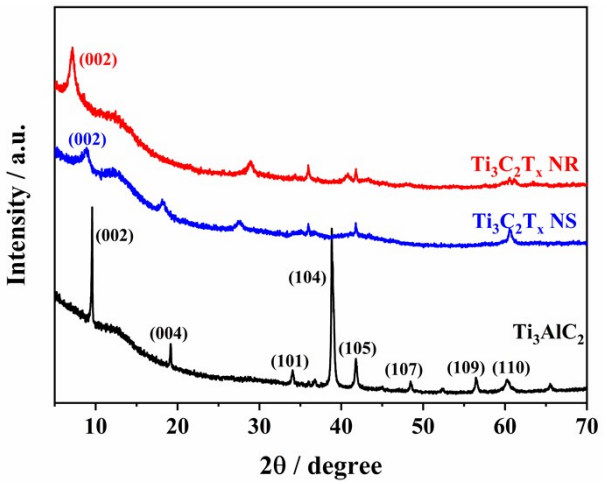

Figure S2. XRD patterns of Ti_3AlC_2, $Ti_3C_2T_x$ NS and $Ti_3C_2T_x$ NR.

The crystallographic structural changes of the pristine Ti_3AlC_2, $Ti_3C_2T_x$ NS and $Ti_3C_2T_x$ NR were investigated by the XRD spectra. As shown in Figure S2, XRD of the Ti_3AlC_2 (MAX phase) pattern was in accordance with the standard spectrum.[1] After the etching process, the most intense diffraction peak e.g., (104), located at $2\theta = 39.0°$, almost disappears, indicating the removal of the Al interlayer. Meanwhile, the (002) peak of $Ti_3C_2T_x$ is broadened and shifts to a low diffraction angle, indicating the substantial expansion of the interlayer distance from Ti_3AlC_2 to $Ti_3C_2T_x$ NS, which we expected. When $Ti_3C_2T_x$ NS was treated with KOH solution via continuous stirring, the 2θ angel of (002) peak was shifted from 8.80° for $Ti_3C_2T_x$ NS to 7.08° for $Ti_3C_2T_x$ NR coupled with a stronger intensity. This was demonstrative of the expansion of interlayer spacing since the rapid adsorption and intercalation of K^+ and OH^- ions into multi layers of $Ti_3C_2T_x$ caused the substantial expansion of interlayer distance.

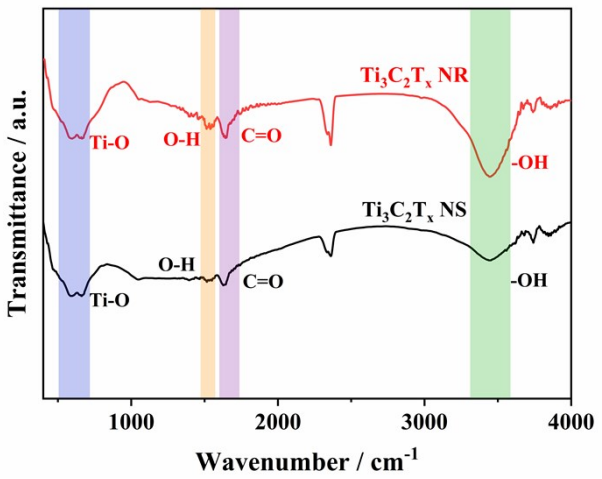

Figure S3. FTIR spectra of $Ti_3C_2T_x$ NS and $Ti_3C_2T_x$ NR.

FT-IR spectroscopy was used to examine the phase and structural properties of obtained materials. The FT-IR spectroscopy spectra (Figure S3) showed several peaks corresponding to vibrations of major surface functional groups; these included Ti-O (~650cm^{-1}), O-H (~1510 cm^{-1}), C=O (~1680 cm–1) and O-H (~3500 cm^{-1}) respectively.

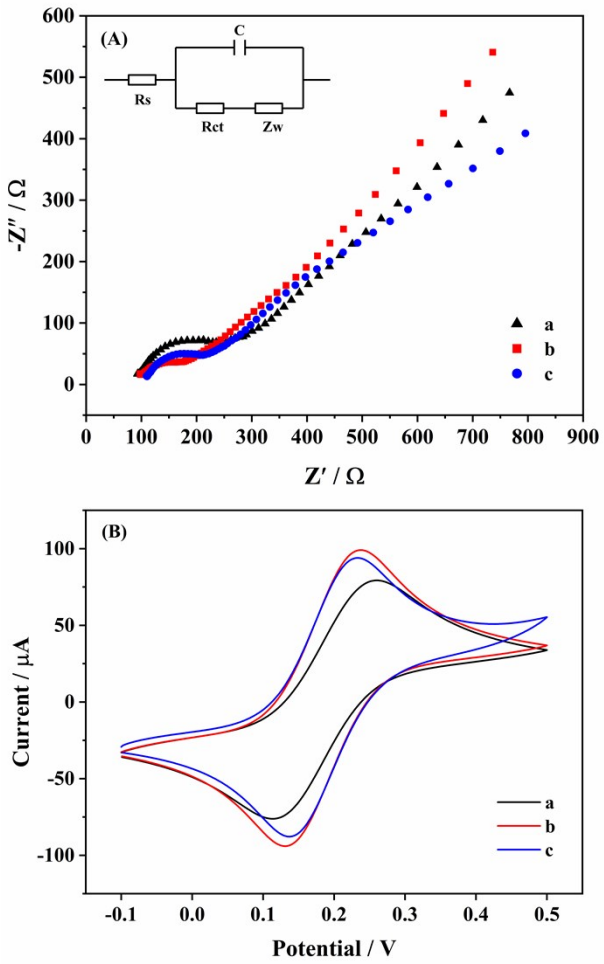

Figure S4. EIS plots (A) and cyclic voltammograms (B) of the bare GCE (a), $Ti_3C_2T_x$ NS/GCE (b) and$Ti_3C_2T_x$ NR/GCE (c) in 0.1 M KCl aqueous solution containing 5.0 mM $[Fe(CN)_6]^{3-/4-}$.The inset (A) is Equivalent circuit for fitting the plots.

The Nyquist plots of GCE, $Ti_3C_2T_x$ NS/GCE and $Ti_3C_2T_x$ NR/GCE was measured in 5.0 mM $[Fe(CN)_6]^{3-/4-}$ solution which contains 0.1 mol L^{-1} KCl. Via fitting the impedance data using Randles equivalent circuit (inset of Figure S4A), the corresponding charge transfer resistance (R_{ct}) values of GCE, $Ti_3C_2T_x$ NS/GCE and $Ti_3C_2T_x$ NR/GCE are 198.1, 85.0 and 125.7 Ω**,** respectively. The resistance values decreased in $Ti_3C_2T_x$ NS/GCE owing to the fast electron transfer property of $Ti_3C_2T_x$. As for $Ti_3C_2T_x$ NR/GCE, the resistance values have increased to a certain extent**.** This is due

to the electrostatic repulsion between $[Fe(CN)_6]^{3-/4-}$ group and the negatively charged hydroxyl group. Meanwhile, the electrode preparation was also studied by cyclic voltammetry (CV) using $[Fe(CN)_6]^{3-/4-}$ as a probe (Figure S4B). As shown in Figure S4B, a pair of well-defined redox peaks appears at GCE. After modifying with Ti_3C_2Tx NS, the peak currents enhanced remarkably at $Ti_3C_2T_x$ NS/GCE and ΔEp becomes smaller, suggesting that $Ti_3C_2T_x$ MXene has high electronic conductivity and surface area. As for $Ti_3C_2T_x$ NR/GCE, the redox peak currents decreased, consistent with it's the resistance value.

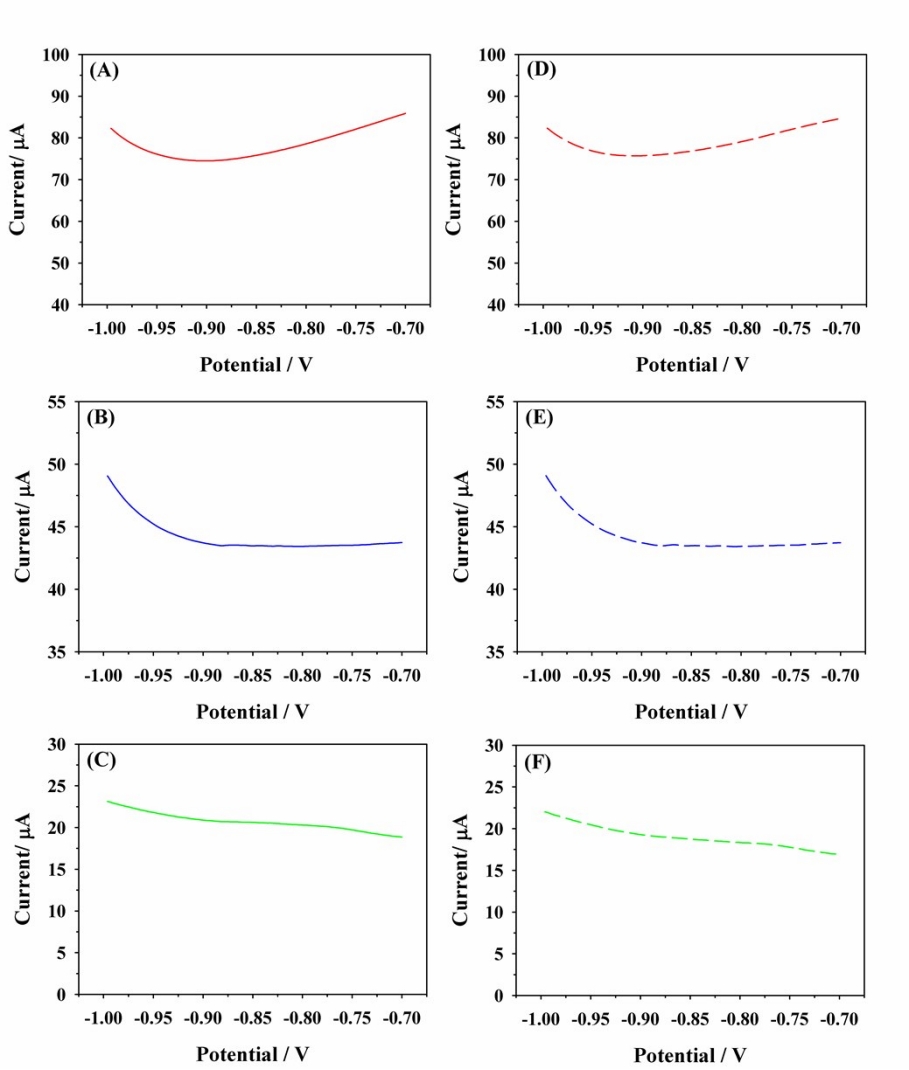

Figure S5. DPV curves of the GO/GCE (A), CB/GCE (B) and oxidized MWCNTs/GCE (C) after immersing in 2.0 μM Cd^{2+} solution; the background current response of GO/GCE (D), CB/GCE (E) and oxidized MWCNTs/GCE (F).

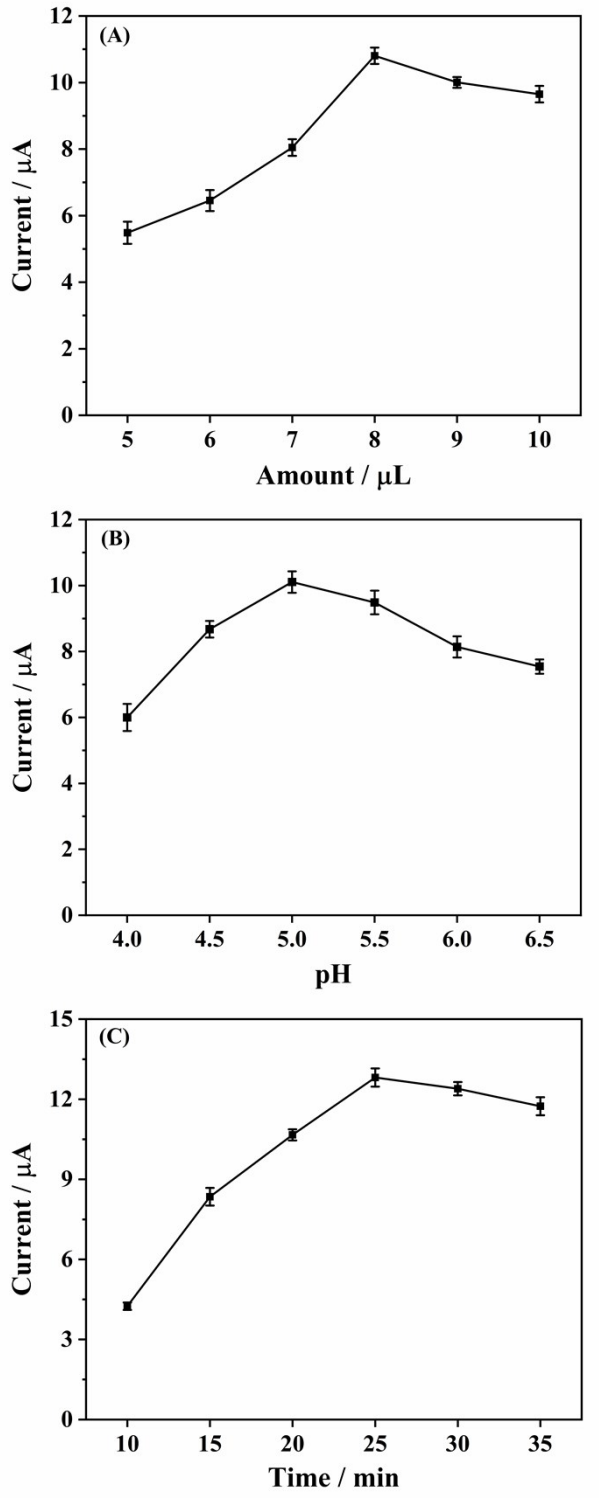

Figure S6. The influence of amount of $Ti_3C_2T_x$ NR (A), the pH value of PBS (B) and accumulation time(C) on the DPV peak currents of Cd^{2+} at $Ti_3C_2T_x$ NR/GCE in 0.1 M PBS.

Figure S6A shows the effects of the amount of $Ti_3C_2T_x$ NR (5.0 to 10.0 μL) on the GCE surface towards the response current, the achieved results show that the optimized parameter

was 8.0 μL. Then, the influence of the pH value of PBS on the oxidation peak currents of Cd^0 was examined from 4.0 to 6.5 (Figure S6B), it can be found the peak currents increase with the increase of pH from 4.0 to 5.0, which can be attributed to the protonation of active groups at lower pH values and the decreasing their absorption ability to Cd^{2+}. However, the peak current begins to decrease when pH value increases from 5.0 to 6.5, which may be attributed to the formation of metal ions hydroxide compounds and the inhibition of their accumulation. Therefore, the pH value of PBS at 5.0 was selected throughout the work. Furthermore, the effect of self-reduction time towards the DPV current was studied also (Figure S6C). It's noted the DPV currents increase with the increase of the time, and the maximum was obtained at 25 min, suggesting that the longer time is benefit for the accumulation and self-reduction of Cd^{2+} on the $Ti_3C_2T_x$ NR/GCE surface. However, when the time exceeds 25 min, the peak current decreased slightly resulted from the active sites saturation; hence 25 min was used for the detection of Cd^{2+}.

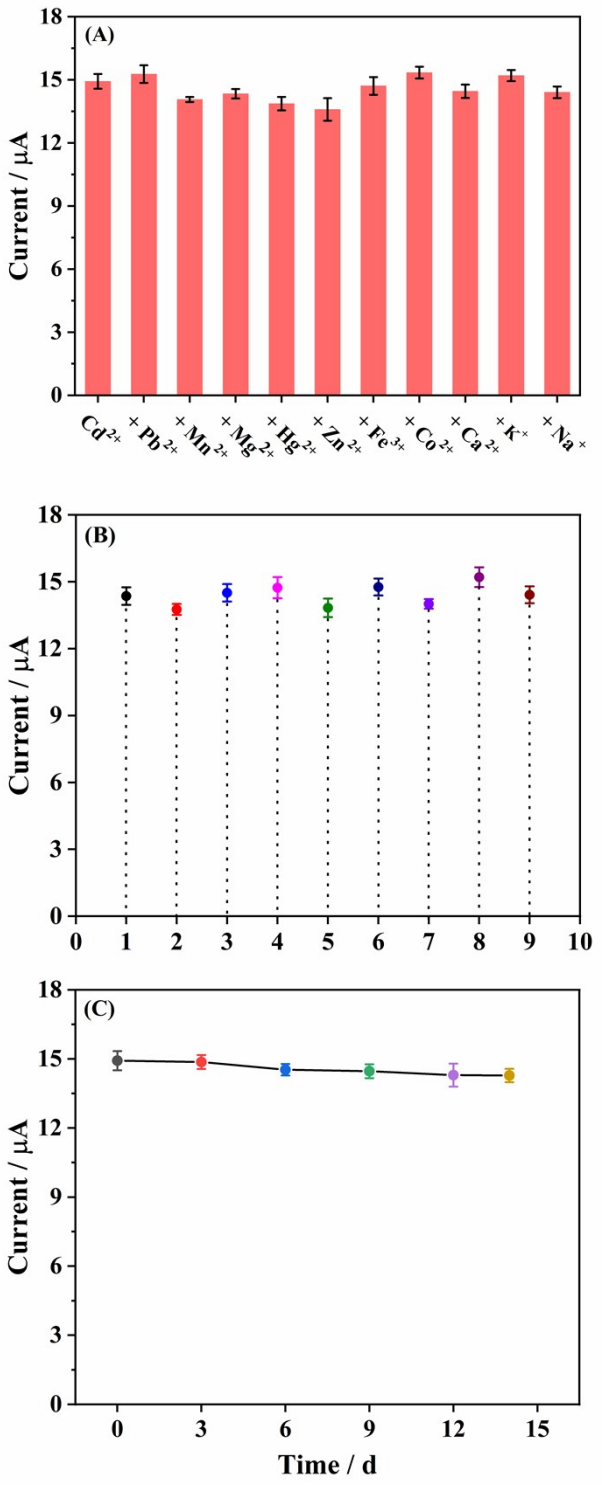

Figure S7. The peak current values of 1.0 μM Cd^{2+} containing various inorganic ions (A); the peak current values of 1.0 μM Cd^{2+} at 9 independently fabricated electrodes (B); the stability test of the fabricated electrodes in two weeks (C).

Table S1. Comparison of $Ti_3C_2T_x$ NR/GCE and the reported electrodes over the last three years for electrochemically detecting Cd^{2+}.

*Electrodes	Electroreduction		Linear range / μM	LOD / nM	Sensitivity μA /μM	Refer.
	Potential/ V	Time/ s				
GA-UiO-66-NH_2/GCE	-1.30	250	0.01-1.5	9.0	0.2716	2
trGNO/Fc-NH_2-UiO-66/GCE	-1.20	310	0.01-2.0	8.5	/	3
PG/GCE	-0.90	1600	0.25-5.5	15.0	-7.291	4
a-g-C_3N_4/GCE	-1.5	150	0.05-0.7	3.9	22.668	5
Nafion/BiSn@C/GCE	-1.2	300	0.01-30.0	3.0	2.495	6
Nano-PPCPE	-1.0	300	0.1-3.0	78.0	2.73	7
NH_2-MIL-88(Fe)-rGO/GCE	-1.0	240	0.005-0.3	4.9	190.36	8
ZJU-77/Nafion/GCE	-1.4	140	0.0-0.53	1.0	30.26	9
Sb_2O_3/MWCNTs/CPE	-1.0	600	0.72-1.04	100.0	26.9	10
CB/PLAprinted electrode	-1.0	200	0.27-2.4	26.0	20.6	11
NH_2-MIL-88(Fe)-rGO/GCE	-1.00	240	0.005-0.3	4.9	190.36	8
F@SnO_2/T/RGO/GCE	-0.60	120	0.02-2.0	5.0	9.0	12
NG/GCE	-1.10	300	0.05-9.0	30.0	2.842	13
MgFe-LDH/graphene/GCE	-1.10	180	0.1-1.0	4.7	26.15	14
GSH@Fe_3O_4/MGCE	-1.4	210	0.0044-0.89	1.5	8.40752	15
$Ti_3C_2T_x$ NR/GCE	No requirement		0.005-3.0	0.96	14.508	This work

*GA, graphene aerogel; UiO-66-NH_2, the metal-organic framework crystal; a-g-C_3N_4, activated graphitic carbon nitride; BiSn@C, carbon supported BiSn alloy nanoparticles; nano-PPCPE, nano-porous pseudo carbon paste electrode; MWCNTs, multiwall carbon nanotube; CPE, carbon paste electrodes; CB, carbon black; PLA, polylactic acid; trGNO, thermally reduced graphene oxide; Fc-NH2-UiO-66, ferrocenecarboxylic acid functionalized metal-organic framework; PG, poly(L-glutamic acid) and graphene oxide composite; NH_2-MIL-88(Fe), a kind of metal-organic frameworks; rGO, reduced graphene oxide; F, fluorine; T, 2-aminobenzothiazole and 2-amino-4-thiazoleacetic acid; RGO, reduced graphene oxide; NG, N-doped graphene; MgFe-LDH, hierarchical MgFe-layered double hydroxide microspheres; GSH@Fe_3O_4, glutathione functionalized iron oxide nanocomposite; MGCE, magnetic glassy carbon electrode.

References

1. X. Wang,Y. Zhou, *J. Mater. Chem.*, 2002, **12**, 455-460.

2. M. Lu, Y. Deng, Y. Luo, J. Lv, T. Li, J. Xu, S.W. Chen,J. Wang, *Anal. Chem.*, 2019, **91**, 888-895.

3. X. Wang, Y. Qi, Y. Shen, Y. Yuan, L. Zhang, C. Zhang,Y. Sun, *Sens. Actuators, B*, 2020, **310**, 127756.

4. J. Song, P. Ran, F. Mo, J. Wu,Y. Fu, *J. Electrochem. Soc.*, 2019, **166**, B426-B431.

5. Y. Liu, G.-L. Wen, X. Chen, R. Weerasooriya, Z.-Y. Hong, L.-C. Wang, Z.-J. Huang,Y.-C. Wu, *Anal. Bioanal. Chem.*, 2020, **412**, 343-353.

6. Y. Chen, D. Zhang, D. Wang, L. Lu, X. Wang,G. Guo, *Talanta*, 2019, **202**, 27-33.

7. Y. Liu, T. Li, C. Ling, Z. Chen, Y. Deng,N. He, *Chin. Chem. Lett.*, 2019, **30**, 2211-2215.

8. S. Duan,Y. Huang, *J. Electroanal. Chem.*, 2017, **807**, 253-260.

9. Y. Li, T. Xia, J. Zhang, Y. Cui, B. Li, Y. Yang,G. Qian, *J. Solid State Chem.*, 2019, **275**, 38-42.

10. T.L. Hai, L.C. Hung, T.T.B. Phuong, B.T.T. Ha, B.-S. Nguyen, T.D. Hai,V.-H. Nguyen, *Microchem. J.*, 2020, **153**, 104456.

11. D.P. Rocha, A.L. Squissato, S.M. da Silva, E.M. Richter,R.A.A. Munoz, *Electrochim. Acta*, 2020, **335**, 135688.

12. X. Cui, X. Fang, H. Zhao, Z. Li,H. Ren, *Colloids Surf., A*, 2018, **546**, 153-162.

13. H. Xing, J. Xu, X. Zhu, X. Duan, L. Lu, W. Wang, Y. Zhang,T. Yang, *J. Electroanal. Chem.*, 2016, **760**, 52-58.

14. Y. Ma, Y. Wang, D. Xie, Y. Gu, X. Zhu, H. Zhang, G. Wang, Y. Zhang,H. Zhao, *Chem. Eng. J.*, 2018, **347**, 953-962.

15. M. Baghayeri, A. Amiri, B. Maleki, Z. Alizadeh,O. Reiser, *Sens. Actuators, B*, 2018, **273**, 1442-1450.

Table S2. The determination of Cd^{2+} in real samples

Samples	Spiked (μM)	Found (μM)	Recovery (%)	RSD (%)
Tap water	0.5	0.47	94.0	4.24
	1.0	1..03	103	3.56
	2.0	1.89	94.5	2.31
Lake water	0.5	0.53	106	4.69
	1.0	1.07	107	3.44
	2.0	2.13	106.5	4.15